İSTANBUL UNIVERSITY CERRAHPAŞA

ORIGINAL ARTICLE
Electrica 2024; 24(2): 450-462

Reduced-Order Fractionalized Controller for Disturbance Compensation Based on Direct Torque Control of DSIM With Less Harmonic

Sifelislam Guedida[1], Bekheira Tabbache[1], Kamal Nounou[1], Abdelhakim Idir[2]

[1]UER ELT, Ecole Militaire Polytechnique, Algiers, Algeria
[2]Department of Electrical Engineering, University Mohamed Boudiaf of M'sila, M'sila, Algeria

Cite this article as: S, Guedida. B, Tabbache, K, Nounou and A, Idir. "Reduced-order fractionalized controller for disturbance compensation-based on direct torque control of DSIM with less harmonic," *Electrica*, 24(2), 450-462, 2024.

ABSTRACT

This paper proposes a new design of a speed regulator loop based on a reduced-order fractionalized proportional-integral controller (ROFrPI) for direct torque control (DTC) of a dual-star induction motor drive with less harmonics in order to improve speed and electromagnetic torque responses. The developed approach employs a modified switching table of DTC to control the stator flux in the harmonic subspace and eliminate circulation currents and therefore obtain purely sinusoidal current form. The effectiveness of the proposed configuration has been tested under various operating conditions by evaluating transient speed and torque responses. Moreover, a comparative investigation has been carried-out to evaluate the performance of the proposed ROFrPI controller for five fractional-order integrator values using the Matsuda approximation. For this, the obtained results demonstrate that the proposed controllers in the speed regulator loop exhibit high performance and better resilience than the conventional controller in terms of overshoot, settling time, and rise time for speed and torque.

***Index Terms*—**Current harmonics, direct torque control (DTC), dual-star induction motor (DSIM), fractionalized proportional-integral-derivative (PID), reduced order approximation

I. INTRODUCTION

Recently, multiphase electric motor drives have become of interest in many industry applications due to their benefits such as high reliability, fault tolerance, and medium torque variation, compared to simple three-phase drives. Therefore, dual-star induction motor (DSIM) is widely used in electric powertrains of railways, aircraft, ships, electric braking systems, and wind power generation, due to its advantages such as the suppression of sixth harmonic torque pulsation [1–6]. The DSIM machine consists of two three-phase stator stars shifted by 30 degrees electrically, while the two neutral points are isolated [7–10]. However, the DSIM suffers from harmonic currents. For this reason, the classical model approach based on two shifted stars of three-phase windings cannot control the harmonic components [3, 6–8]. In order to control the harmonic components, reference [6] proposes the vector space decomposition (VSD) technique based on the decomposition of the voltage, the current, and the flux of DSIM into three subspaces (α–β), (x–y), and (o1–o2), in order to visualize the subspace associated with harmonic components.

In terms of control, many advanced control strategies have been developed, such as field-oriented control (FOC) and model predictive control [6, 11]. Regarding the robustness under parameter system disturbances, simple structure, direct torque control (DTC) becomes the more adopted approach to control the DSIM [12-14]. However, the classical DTC based on the proportional integrator regulator of the speed loop control (DTC-PI) can generate a large harmonic current caused by the non-zero mean voltage in subspace (x-y) [13–15]. So, the lack of control of harmonic currents in the (x–y) subspace increase the total harmonic distortion (THD) significantly. In order to minimize harmonic currents, the authors of references [16-19] propose a solution for five-phase and six-phase induction motors drives. It is based on a modified switching table of the DTC where the selection of the appropriate voltage vector depends on the position of the stator flux in the (x–y) subspace.

Corresponding author:
Sifelislam Guedida

E-mail:
guedida.sifelislam@gmail.com

Received: December 26, 2023

Revision Requested: February 9, 2024

Last Revision Received: March 28, 2024

Accepted: April 7, 2024

Publication Date: May 17, 2024

DOI: 10.5152/electrica.2024.23194

In addition, the DTC based on virtual voltage vectors in which two voltage vectors are applied at each sampling time can lead to a zero voltage value in the subspace (x–y) and significantly reduce harmonic currents [9, 19-23]. However, in this method, the average switching frequency of the inverter power switches can increase more than two times and present a difficulty in hardware implementation. This paper presents a modified DTC method (MDTC-PI) based on a two-step approach to control stator flux in (x–y) subspace in order to minimize the THD of harmonic currents.

On the other hand, proportional integral (PI) controllers are widely used in various industry fields due to the simplicity of implementation and their robustness. However, PI controllers present limitations under system parameter disturbances [24, 25]. In addition, the PI controller used in the DTC generates the torque reference, which is sensitive to speed and torque variations. Therefore, the fractional-order controller can improve the dynamic performance of DTC in system parameter disturbance conditions.

In multiphase electric drive systems, fractional-order controllers can offer better performance than conventional PID controllers [26, 27]. Moreover, high performance of the fractional-order PI regulators can also be obtained by optimizing the gains of these regulators using genetic optimization algorithms [28]. In addition, the PI controller can be fractionalized and offer an improvement over the various types of fractional-order controllers [29-31].

In this context, this paper presents an improvement of speed and torque response by using a fractionalized PI controller (FrPI) of the DTC for the DSIM. The Matsuda approximation approach is used to transform the fractional-order transfer function of the FrPI into an integer order. Furthermore, the paper proposes five approaches based on the reduced-order FrPI controller (ROFrPI) for each value of the fractionalized order integrator, in order to minimize memory size and facilitate implementation of the modified DTC of DSIM (hereinafter referred to as modified direct torque control (MDTC)-ROFrPI).

The structure of this paper is as follows: firstly, modeling of the DSIM based on the VSD technique is presented. The principles of classical DTC (DTC-PI) are given in the next section. The impact of voltage vectors on the harmonic current minimization of the modified MDTC-PI is also treated. The next sections focus on fractional calculus and the proposed MDTC-ROFrPI, which is based on the reduced-order FrPI. Finally, extensive simulations are carried out to prove the efficiency of the proposed method.

II. DEVELOPED DIRECT TORQUE CONTROL TECHNIQUES OF DSIM

A. DSIM model

In the model of the DSIM fed by a six-phase voltage source inverter (see Fig. 1), the following assumptions have been taken into account: the DSIM windings are sinusoidally distributed, the flux path is linear, mutual leakage inductances are neglected, and a unitary rotation ratio between stator and rotor is assumed [7–8]. An approach was developed by [6] using a transformation matrix called VSD, according to which the six-dimensional origin space of the double-star machine can be decoupled into three subspaces (α–β), (x–y), and (o_1–o_2). The fundamental variables of the machine, such as voltage, current, and flux, which are related to the electromechanical conversion of energy, as well as the harmonics of order $h = 12n \pm 1$, ($n = 1, 2, 3, ...$), are projected into (α–β) space. Harmonic components projected into (x–y) subspace are unrelated to electromechanical energy conversion. These harmonics correspond to orders $h = 6n \pm 1$ ($n = 1, 3, 5, ...$) such as 5th, 7th, 17th, 19th, ..., which are difficult to control. When neutral points (N1 and N2) are isolated, null sequences with $h = 3n$ ($n = 1, 3, 5, ...$) that are projected into (o_1–o_2) space are not considered. The decomposition matrix [T] is presented in equation 1 as follows:

$$[T] = \frac{1}{\sqrt{3}} \begin{bmatrix} 1 & -\frac{1}{2} & -\frac{1}{2} & \frac{\sqrt{3}}{2} & -\frac{\sqrt{3}}{2} & 0 \\ 0 & \frac{\sqrt{3}}{2} & -\frac{\sqrt{3}}{2} & \frac{1}{2} & \frac{1}{2} & -1 \\ 1 & -\frac{1}{2} & -\frac{1}{2} & -\frac{\sqrt{3}}{2} & \frac{\sqrt{3}}{2} & 0 \\ 0 & -\frac{\sqrt{3}}{2} & \frac{\sqrt{3}}{2} & \frac{1}{2} & \frac{1}{2} & -1 \\ 1 & 1 & 1 & 0 & 0 & 0 \\ 0 & 0 & 0 & 1 & 1 & 1 \end{bmatrix} \quad (1)$$

The final model of the DSIM as a function of voltages, currents, stator flux, and torque can be expressed in the three subspaces (α–β), (x–y), and (o1–o2) as follows, using the transformation matrix (1):

$$V_{s\alpha\beta} = R_s I_{s\alpha\beta} + \frac{d\Psi_{s\alpha\beta}}{dt} \quad (2)$$

$$\Psi_{s\alpha\beta} = L_{s\alpha\beta} I_{s\alpha\beta} + \Psi_{r\alpha\beta} \quad (3)$$

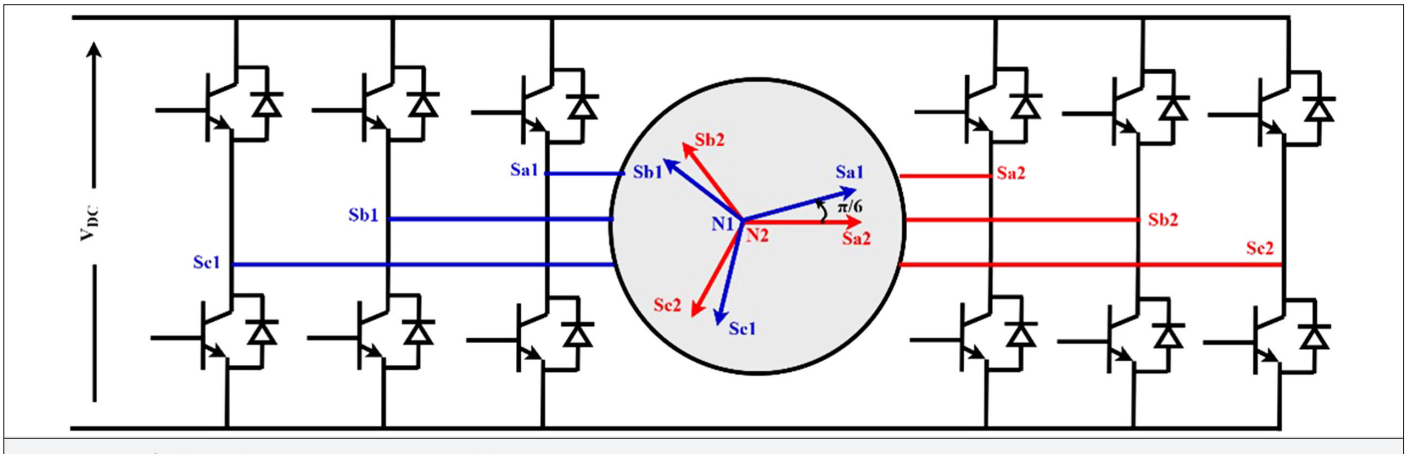

Fig. 1. DSIM fed by voltage source inverter and drives.

$$V_{sxy} = R_s I_{sxy} + \frac{d\Psi_{sxy}}{dt} \quad (4)$$

$$\Psi_{sxy} = L_{ls} I_{sxy} \quad (5)$$

$$V_{so1o2} = R_s I_{so1o2} + \frac{d\Psi_{so1o2}}{dt} \quad (6)$$

$$\Psi_{so1o2} = L_{ls} I_{so1o2} \quad (7)$$

$$T_e = p\left(\Psi_{s\alpha} I_{s\beta} - \Psi_{s\beta} I_{s\alpha}\right) \quad (8)$$

where:

$V_{s\alpha\beta}$, V_{sxy}, and V_{solo2} are the stator voltages in the (α–β), (x–y), and (o1–o2) subspaces, respectively.

$I_{s\alpha\beta}$, I_{sxy}, and I_{solo2} are the stator currents in the (α–β), (x–y), and (o1–o2) subspaces, respectively.

$\psi_{s\alpha\beta}$, ψ_{sxy}, and ψ_{solo2} are the stator flux in the (α–β), (x–y), and (o1–o2) subspaces, respectively.

L_m, L_{ls}, and $L_{s\alpha\beta} = L_{ls} + 3L_m$ are the magnetizing inductance, leakage inductance, and stator inductance, respectively.

P, R_s, and T_e: are number of pole pairs, stator resistance, and electromagnetic torque, respectively.

B. Modified DTC

Due to the configuration of the six-leg inverter, it can generate 64 possible switching combinations, i.e., 64 voltage vectors. By neglecting the voltage vectors that are defined by the combination ([1 1 1 Sa2 Sb2 Sc2], [0 0 0 Sa2 Sb2 Sc2], [Sa1 Sb1 Sc1 1 1 1], [Sa1 Sb1 Sc1 0 0 0], (Sa1, Sb1, Sc1, Sa2, Sb2, and Sc2: 1 or 0, respectively)), the voltage vectors in the two spaces (α–β) and (x–y) are presented in Fig. 2 according to equations 9 and 10, as follows:

$$V_{s\alpha\beta} = V_{s\alpha} + jV_{s\beta} = \frac{1}{3}(V_{sa1} + aV_{sb1} + a^4 V_{sc1} + a^5 V_{sa2} + a^8 V_{sb2} + a^9 V_{sc2}) \quad (9)$$

$$V_{sxy} = V_{sx} + jV_{sy} = \frac{1}{3}(V_{sa1} + a^5 V_{sb1} + a^8 V_{sc1} + aV_{sa2} + a^4 V_{sb2} + a^9 V_{sc2}) \quad (10)$$

Fig. 2 shows the voltage vectors used in this paper in the two subspaces (α–β) and (x–y). It is clear that the voltage vectors are aligned in the same line and grouped into three dodecagons (D_S, D_M, and D_L), and their amplitude in subspace (α–β) is as follows:

$$\begin{cases} V_L = 2M\cos 15^0 = \dfrac{\sqrt{6}+\sqrt{2}}{2} M \\ V_M = 2M\cos 45^0 = \sqrt{2} M \\ V_S = 2M\cos 75^0 = \dfrac{\sqrt{6}-\sqrt{2}}{2} M \end{cases} \quad (11)$$

where M is $\frac{2}{3} V_{dc}$

Fig. 3 shows a diagram of the DTC-PI for DSIM, based on a conventional PI controller for the speed loop. The principle is similar to that of the single three-phase machine. The (α–β) space can be divided into 12 sectors according to the extended voltage vectors that are chosen from the DL dodecagon in order to maximize the utilization rate of the DC power supply, as illustrated in Fig. 4. When the stator flux is in one of these sectors, and depending on the output of the torque hysteresis regulators and stator flux, an appropriate voltage vector is selected by means of a switching table, as mentioned in Table I.

The DTC-PI applied to the DSIM drive system is very easy to use due to its simple structure. However, as indicated by equations 4 and 5, the main drawback is the lack of control over the stator flux in the (x–y) subspace, resulting in significant harmonic currents.

From equation (5), it is clear that the harmonic components depend on the stator flux in subspace (x–y). Therefore, to reduce harmonic currents, it is necessary to minimize stator fluxes in subspace (x–y). The authors of the papers [16–18, 23] found an effective solution to minimize and control harmonic currents in the (x–y) subspace. In

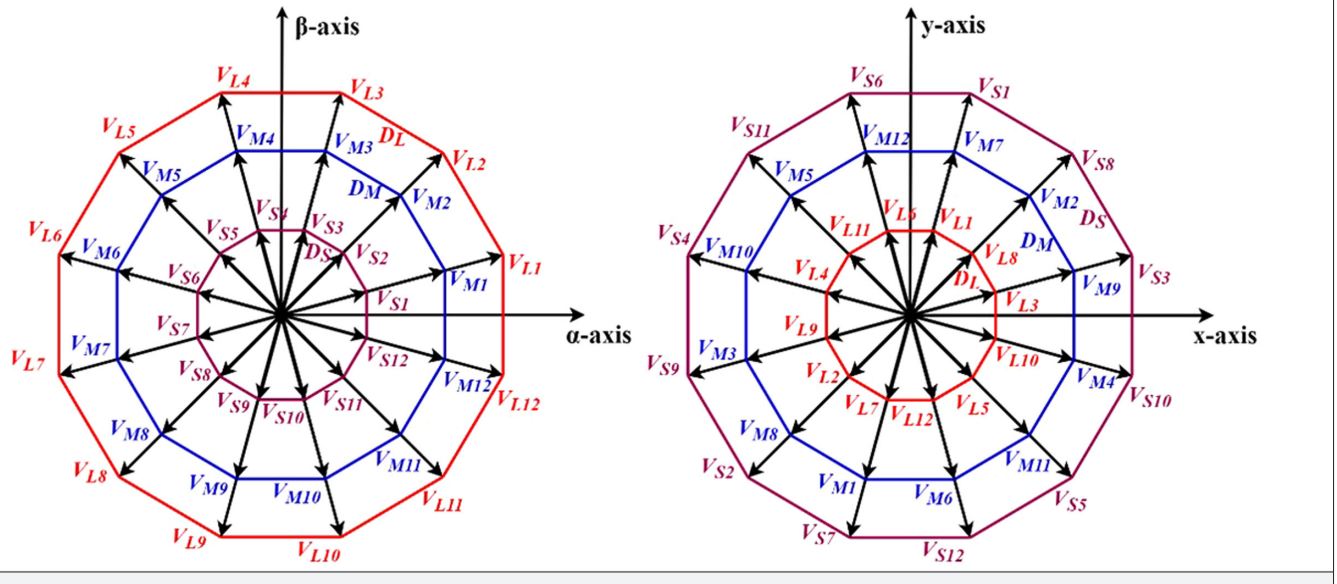

Fig. 2. Inverter voltage vectors. (a) α–β subspace and (b) x–y subspace.

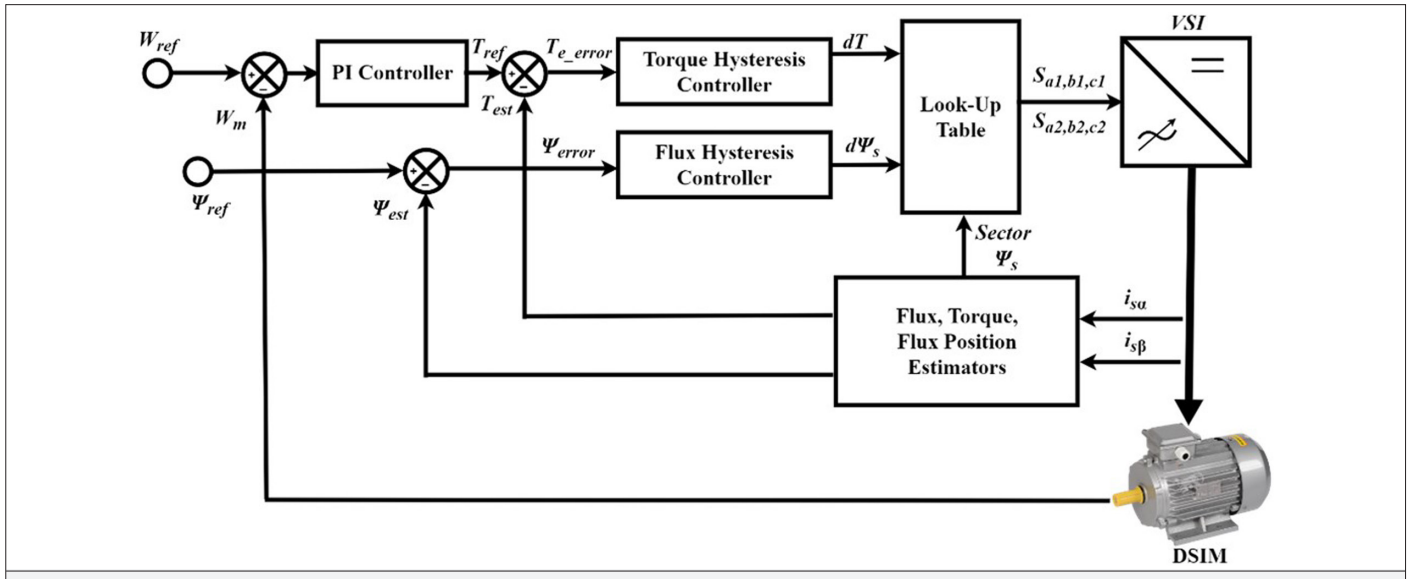

Fig. 3. Diagram of the classical DTC for DSIM.

this paper, a similar technique is applied to the DSIM with the aim of minimizing circulating currents.

As previously mentioned, the three voltage vectors V_L, V_M, and V_S point in the same direction and have a similar effect in subspace (α–β). However, for example, Fig. 5 clearly shows that in subspace (x–y), vectors V_{L3} and V_{S3} always point in the same direction, while vector V_{M3} points in the opposite direction. Consequently, the stator flux variation in subspace (x–y) can be controlled by the suitable voltage vectors depending on the stator flux position for each sector.

Fig. 6 shows the MDTC-PI diagram, similar to the paper [16, 23], for the DSIM, which features modifications compared to the DTC-PI. The

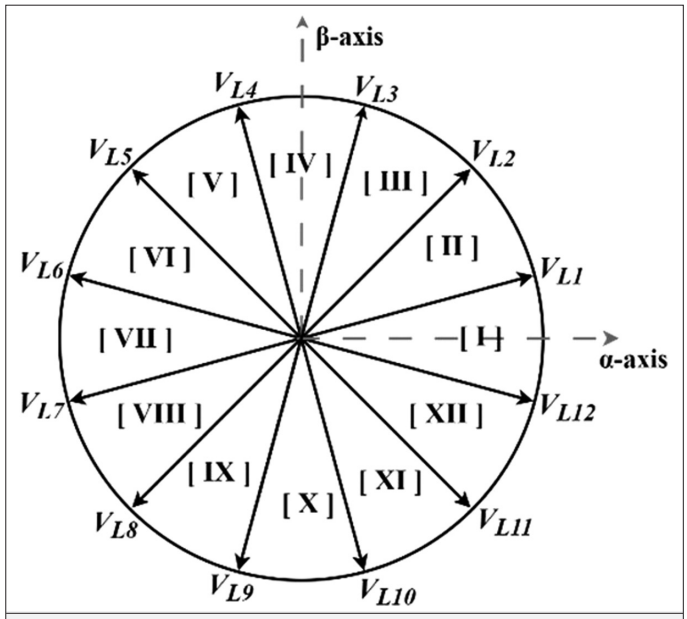

Fig. 4. Definition of 12 large voltage vectors in (α–β) subspace.

TABLE I. SWITCHING TABLE FOR DTC-PI

ψ_s in Sector k (1:12)	$\Delta T_e = 1$	$\Delta T_e = -1$	$\Delta T_e = 0$
$\Delta\psi_s = 1$	V_{k+2}	V_{k-3}	V_{zero}
$\Delta\psi_s = -1$	V_{k+3}	V_{k-4}	V_{zero}

ψ_s: Stator flux, T_e : Electromagnetic torque, V_k : Appropriate voltage vector.

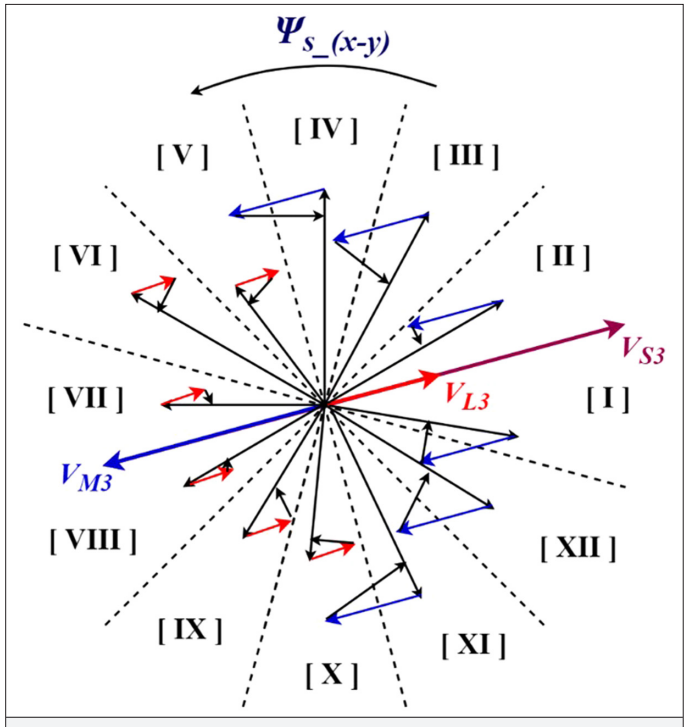

Fig. 5. Effect of voltage vectors V_{L3}, V_{M3}, and V_{S3} on stator flux variation in subspace (x–y).

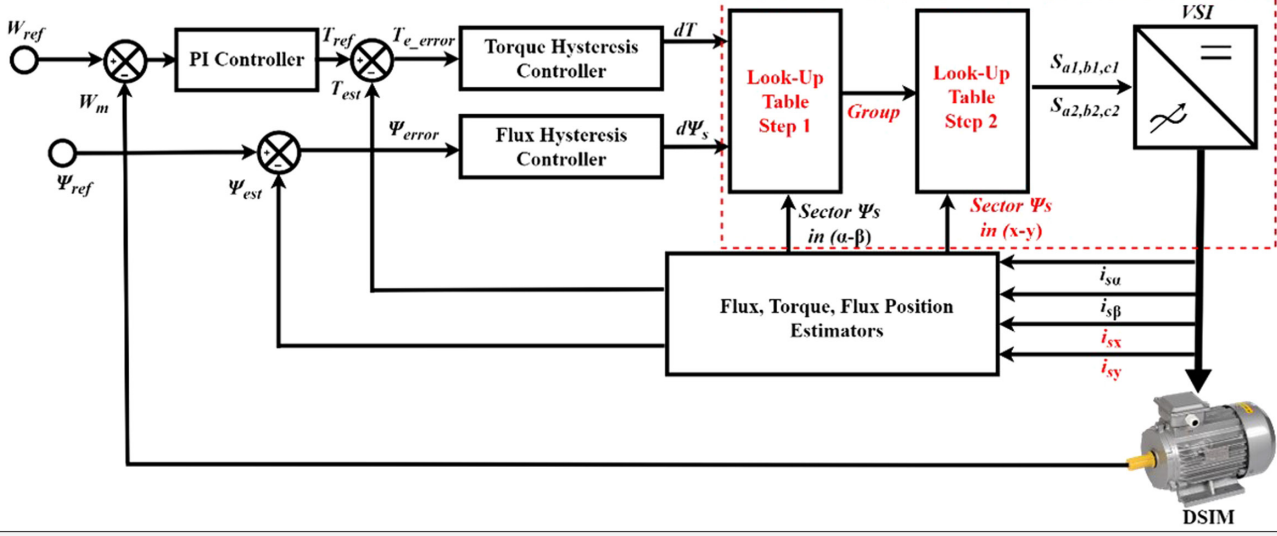

Fig. 6. Diagram of the Modified DTC for DSIM.

principle of harmonic current minimization is based on a two-step process. Clearly, this principle necessitates the addition of a stator flux estimator in subspace (x–y), as well as a second switching table. As a result, the advantages of DTC-PI, such as its simple structure and robustness, are still preserved.

It is clear that the first step in MDTC-PI is to preserve the principle of DTC-PI for selecting the appropriate group depending on the output of the hysteresis regulators and the position of the stator flux in subspace (α–β) using a switching table similar to that of DTC-PI. However, if the group is selected, the second step relies on the position of the stator flux in the (x–y) subspace with a second switching table that selects the suitable voltage vectors based on the sector k where the stator flux is located in the (x–y) subspace. To clarify the definition of sectors in the two spaces as a function of sector k, it is as follows:

$$-\frac{\pi}{12}+\frac{\pi}{6}(k-1)\le\theta_{s\alpha\beta},\theta_{sxy}<\frac{\Pi}{12}+\frac{\Pi}{6}(k-1),k=1,2,.....12 \tag{12}$$

In general, MDTC-PI has demonstrated its capacity to minimize harmonic currents, as well as to slightly reduce DC power supply compared to DTC-PI, due to the selection of voltage vectors, as shown in equation 13. In addition, it maintains its reliability in the face of external disturbances, which will be confirmed by simulation results.

$$\eta=\frac{|V_L|\times T_s/2+|V_M|\times T_s/2}{|V_L|\times T_s}\times100\%=\frac{\left(\sqrt{6}+\sqrt{2}/2\right)M+\sqrt{2}M}{2\times\left(\sqrt{6}+\sqrt{2}/2\right)M}\times100\%=86.60\% \tag{13}$$

III. PROPOSED DTC METHOD BASED ON FRACTIONALIZED CONTROLLER

A. Fractional Calculus Principle

Fractional calculus is an extension of integration and derivation to the non-integer fundamental operator ${}_{a}D_{t}^{\alpha}$, where α and t are the limits of the operation. Integration and differentiation are integrated into the generalized fundamental operator, which is defined as follows:

$${}_{a}D_{t}^{\alpha}=\begin{cases}\dfrac{d^{\alpha}}{dt^{\alpha}}, R(\alpha)>0\\ 1, R(\alpha)=0\\ \displaystyle\int_{a}^{t}(d\tau)^{-\alpha}, R(\alpha)<0\end{cases} \tag{14}$$

α is the order of the fractional operator, while the real part of α is represented by R(α). Integration is indicated by a negative sign and derivation by a positive sign [32].

The Grunwald–Letnikov definition is given as follows:

$${}_{a}D_{t}^{\alpha}f(t)=\lim_{h\to0}\frac{1}{h^{\alpha}}\sum_{r=0}^{\frac{(t-a)}{h}}(-1)^{r}\binom{\alpha}{r}f(t-rh) \tag{15}$$

where $\omega_r^{(\alpha)}=(-1)^r\binom{\alpha}{r}$ represent the coefficients of the polynomial $(1-z)^{\alpha}$.

The coefficients can also be determined recursively, from:

$$\omega_0^{(\alpha)}=1,\omega_r^{(\alpha)}=\left(1-\frac{\alpha+1}{r}\right)\omega_{r-1}^{(\alpha)},r=1,2,\ldots \tag{16}$$

The definition of Riemann–Liouville is as follows:

$${}_{a}D_{t}^{-\alpha}f(t)=\frac{1}{\Gamma(\alpha)}\int_{a}^{t}(t-\tau)^{\alpha-1}f(\tau)d\tau \tag{17}$$

where $0<\alpha<1$.

The definition of the Caputo can be found:

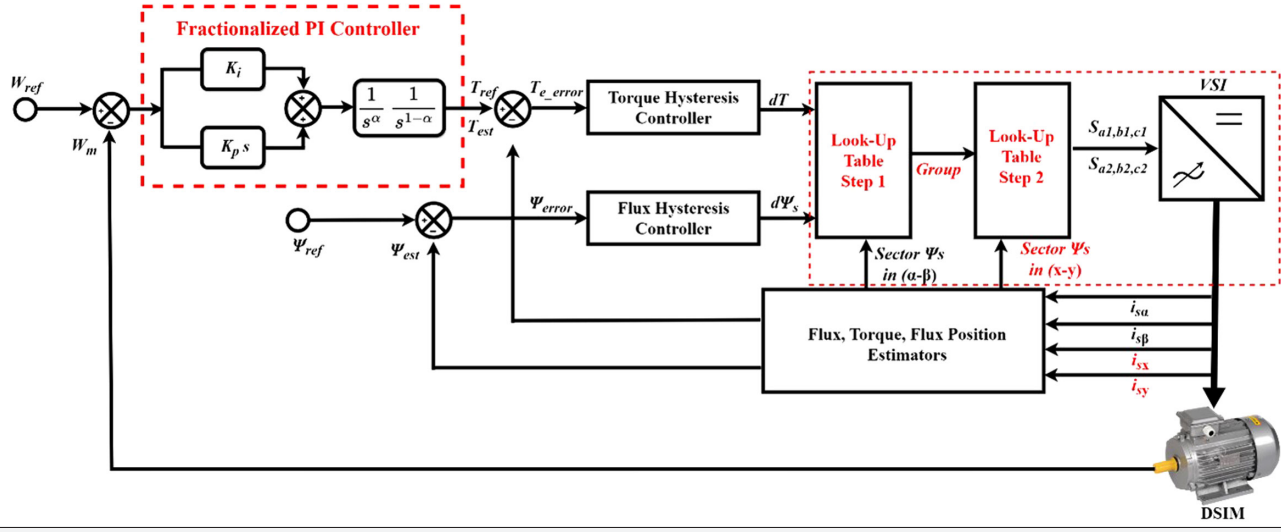

Fig. 7. Diagram of the Proposed DTC for DSIM.

$$0D_t^{-\alpha}y(t)=\frac{1}{\Gamma(1-\gamma)}\int_a^t\frac{y^{(m+1)}(\tau)^{\alpha-1}}{(t-\tau)^{\gamma}}\,d\tau \tag{18}$$

The Riemann–Liouville and Grunwald–Letnikov formulations are equivalent for a wide range of functions encountered in various technical fields and physical systems [33].

In general, fractional controllers have infinite dimension due to the non-integer order of the integration and/or derivation operator. It is therefore necessary to search for approximations of the integer-order for fractional-order systems. However, several studies have proposed finite-dimensional integer-order approximation methods. Matsuda's approximation method is one such method used in this paper, having the particularity of approximating an irrational function by a rational function based on the continued fraction technique [34]. The approximation is defined as follows:

$$G(s)=\alpha_0+\cfrac{s-s_0}{\alpha_1+\cfrac{s-s_1}{\alpha_2+\cfrac{s-s_2}{\alpha_3+\ldots}}} \tag{19}$$

where

$$\alpha_i=v_i(s_i),v_0(s)=G(s),v_{i+1}(s)=\frac{s-s_i}{v_i(s)-\alpha_i}$$

B. Proposed DTC Method Based on ROFrPI Controller

In this section, a modification is incorporated into the DTC speed regulator loop for the DSIM by replacing the integer-order PI controller with a FrPI, as shown in Fig. 7, with the aim of improving speed response and electromagnetic torque in the transient regime, while maintaining the development structure for minimizing and controlling harmonic currents in subspace (x–y). The parameters (k_p, k_i) correspond to the FrPI while α represents the fractional order.

The conventional PI controller is in the following form:

$$G_{PI}(s)=K_p+\frac{k_i}{s} \tag{20}$$

Fig. 8 illustrates the principle of modification of the conventional PI controller by fractionalizing the integration operator $\left(\frac{1}{s}\right)$ into two parts $\left(\frac{1}{s^\alpha}\text{and}\frac{1}{s^{1-\alpha}}\right)$. Equation (21) shows the control law developed, resulting in an improved speed loop regulator.

$$G_{FrPI}(s)=K_p+\frac{k_i}{s}=\frac{K_ps+k_i}{s}=(K_ps+k_i)\frac{1}{s}=(K_ps+k_i)\frac{1}{s^\alpha}\frac{1}{s^{(1-\alpha)}} \tag{21}$$

where $0<\alpha<1$

Therefore, the transfer functions of the speed regulator loop with a FrPI are expressed by the equations from (22) to (26) using the Matsuda approximation. This is done for various values of the fractional integration order $\alpha=0.1$, $\alpha=0.2$, $\alpha=0.3$, $\alpha=0.4$, and $\alpha=0.5$, in a frequency range from $\omega_b=0.001$ rad/s to $\omega_h=1000$ rad/s with a filter order of five ($n=5$), using the parameters $K_p=4.8690$ and $K_i=91.4063$ of the conventional PI controllers.

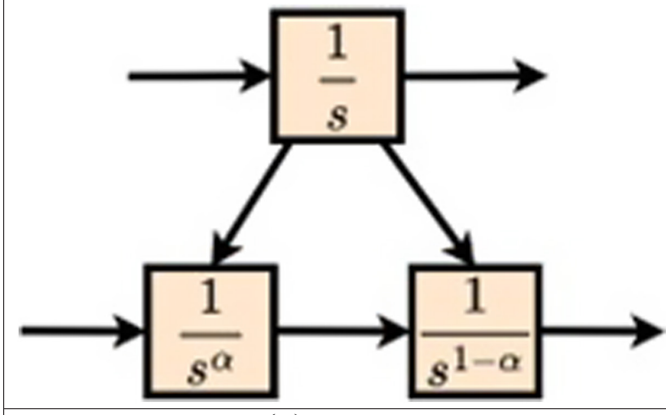

Fig. 8. Integral operator $\left(\frac{1}{s}\right)$ fractionalization.

- Transfer functions of the FrPI controller for $\alpha = 0.1$:

$$G_{FrPI\_0.1}(s)\frac{\begin{array}{c}0.004869s^{11}+6.117s^{10}+1784s^{9}+\\1.346e05s^{8}+3.638e06s^{7}+3.846e07s^{6}+\\1.296e08s^{5}+1.287e08s^{4}+3.082e07s^{3}\\+1.98e06s^{2}+2.842e04s+91.41\end{array}}{\begin{array}{c}s^{10}+310.8s^{9}+2.165e04s^{8}+\\3.36e05s^{7}+1.39e06s^{6}+1.344e06s^{5}+\\3.492e05s^{4}+2.12e04s^{3}+343.1s^{2}\\+1.237s+0.001\end{array}} \quad (22)$$

- Transfer functions of the FrPI controller for $\alpha = 0.2$:

$$G_{FrPI\_0.2}(s)\frac{\begin{array}{c}0.004869s^{11}+5.755s^{10}+1725s^{9}+\\1.272e05s^{8}+3.462e06s^{7}+3.702e07s^{6}+\\1.217e08s^{5}+1.245e08s^{4}+2.89e07s^{3}\\+1.919e06s^{2}+2.671e04s+91.41\end{array}}{\begin{array}{c}s^{10}+292.2s^{9}+2.098e04s^{8}+\\3.151e05s^{7}+1.345e06s^{6}+1.26e06s^{5}+\\3.379e05s^{4}+1.988e04s^{3}+332.5s^{2}\\+1.163s+0.001\end{array}} \quad (23)$$

- Transfer functions of the FrPI controller for $\alpha = 0.3$:

$$G_{FrPI\_0.3}(s)\frac{\begin{array}{c}0.004869s^{11}+5.501s^{10}+1686s^{9}+\\1.221e05s^{8}+3.342e06s^{7}+3.605e07s^{6}+\\1.162e08s^{5}+1.217e08s^{4}+2.757e07s^{3}\\+1.878e06s^{2}+2.551e04s+91.41\end{array}}{\begin{array}{c}s^{10}+279.1s^{9}+2.053e04s^{8}+\\3.005e05s^{7}+1.315e06s^{6}+1.201e06s^{5}+\\3.304e05s^{4}+1.896e04s^{3}+325.4s^{2}\\+1.111s+0.001\end{array}} \quad (24)$$

- Transfer functions of the FrPI controller for $\alpha = 0.4$:

$$G_{FrPI\_0.4}(s)\frac{\begin{array}{c}0.004869s^{11}+5.35s^{10}+1664s^{9}+\\1.191e05s^{8}+3.271e06s^{7}+3.549e07s^{6}+\\1.13e08s^{5}+1.201e08s^{4}+2.678e07s^{3}\\+1.855e06s^{2}+2.48e04s+91.41\end{array}}{\begin{array}{c}s^{10}+271.3s^{9}+2.028e04s^{8}+\\2.919e05s^{7}+1.298e06s^{6}+1.167e06s^{5}+\\3.261e05s^{4}+1.842e04s^{3}+321.4s^{2}\\+1.08s+0.001\end{array}} \quad (25)$$

- Transfer functions of the FrPI controller for $\alpha = 0.5$:

$$G_{FrPI\_0.5}(s)\frac{\begin{array}{c}0.004869s^{11}+5.301s^{10}+1656s^{9}+\\1.181e05s^{8}+3.248e06s^{7}+3.531e07s^{6}+\\1.119e08s^{5}+1.196e08s^{4}+2.652e07s^{3}\\+1.848e06s^{2}+2.457e04s+91.41\end{array}}{\begin{array}{c}s^{10}+268.7s^{9}+2.02e04s^{8}+\\2.891e05s^{7}+1.293e06s^{6}+1.156e06s^{5}+\\3.247e05s^{4}+1.824e04s^{3}+320.1s^{2}\\+1.07s+0.001\end{array}} \quad (26)$$

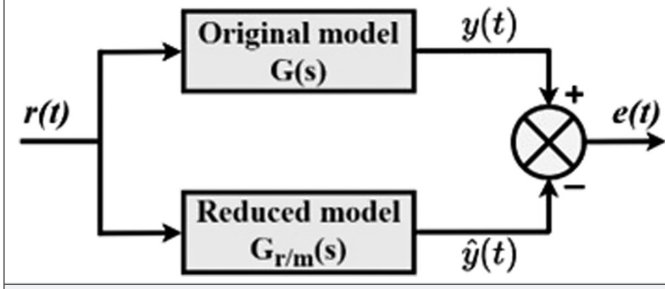

Fig. 9. Error signal for model reduction.

From equations (22) to (26), it is clear that the FrPI, based on Matsuda's approximation method, has a transfer function of order 11, which affects the memory size of the DTC implementation system for the DSIM. Therefore, according to the study [28, 29], it is possible to reduce the order of the filter while maintaining the same performance for the high-level controller. Fig. 9 illustrates the reduction signal error of the model, while the original model is formulated as follows:

$$G(s)=\frac{b_1 s^{n-1}+\ldots+b_{n-1}s+b_0}{s^{n}+a_1 s^{n-1}+\ldots+a_{n-1}s+a_n} \quad (27)$$

The current objective is to identify a low-order approximation model with an integer order, as outlined below [31]:

$$G_{r/m}(s)=\frac{\beta_1 s^{r}+\ldots+\beta_r s+\beta_{r+1}}{s^{m}+\alpha_1 s^{m-1}+\ldots+\alpha_{m-1}s+\alpha_m} \quad (28)$$

The objective function shown below is used to reduce the H2 norm of the minimization error signal.

$$K=\min_{\vartheta}\ \left\|\breve{G}(s)-G_{r/m}(s)\right\|_2 \quad (29)$$

where ϑ represent the parameters to be optimized

$$\vartheta=\left[\beta_1,\ldots,\beta_r,\alpha_1,\ldots,\alpha_m\right] \quad (30)$$

This paper presents a proposed approach, MDTC-ROFrPI, based on the reduced-order FrPI in the speed regulator loop to enhance the dynamic efficiency of DTC-PI. Equations (31) to (35) show the effectiveness of this approach in reducing the order of transfer functions for each value of the proposed fractional order of integration.

- ROFrPI controller for $\alpha = 0.1$:

$$G_{ROFrPI\_0.1}(s)=\frac{6.909s+129.7}{s+0.0003962} \quad (31)$$

- ROFrPI controller for $\alpha = 0.2$:

$$G_{ROFrPI\_0.2}(s)=\frac{9.557s+179.4}{s+0.0009179} \quad (32)$$

- ROFrPI controller for $\alpha = 0.3$:

$$G_{ROFrPI\_0.3}(s)=\frac{12.55s+235.6}{s+0.001515} \quad (33)$$

- ROFrPI controller for $\alpha = 0.4$:

$$G_{ROFrPI\_0.4}(s) = \frac{15.06s + 282.7}{s + 0.002025} \quad (34)$$

- ROFrPI controller for $\alpha = 0.5$:

$$G_{ROFrPI\_0.5}(s) = \frac{16.05s + 301.3}{s + 0.002229} \quad (35)$$

TABLE II. DUAL-STAR INDUCTION MACHINE PARAMETERS

Quantity	Magnitude
Rated speed (ω)	100 rad/s
Number of poles (p)	3
Rated frequency (F)	50 Hz
Stator resistance (R_s)	2.03 Ω
Rotor resistance (R_r)	3 Ω
Leakage inductance (L_{ls})	0.005 H
Magnetizing inductance (L_m)	0.202 H
Stator inductance ($L_{s\alpha\beta}$)	0.217 H

IV. VALIDATION RESULTS AND DISCUSSION

This section examines the effectiveness of the various techniques proposed using the MATLAB/Simulink simulation tool. The specific parameters of the DSIM are presented in Table II. The investigation evaluates the effectiveness of the five proposed DTC techniques based on the FrPI and compares them with the conventional PI controller. Simulations are carried out for different techniques. The gain values of the conventional PI controller and the FrPI are given in the previous section. The electromagnetic torque and stator flux hysteresis regulator bands are set to 0.2 Nm and 0.00125 Wb, respectively, to achieve the desired response.

To prove the effectiveness of the modified DTC for minimizing the harmonic components in the (x–y) subspace, Figs. 10–12 present the simulation results of the DTC-PI and MDTC-PI of the DSIM drive in steady state. The rotor speed is set at 100 rad/s, while the load torque is 20 Nm with a reference stator flux of 0.7 Wb. As shown in

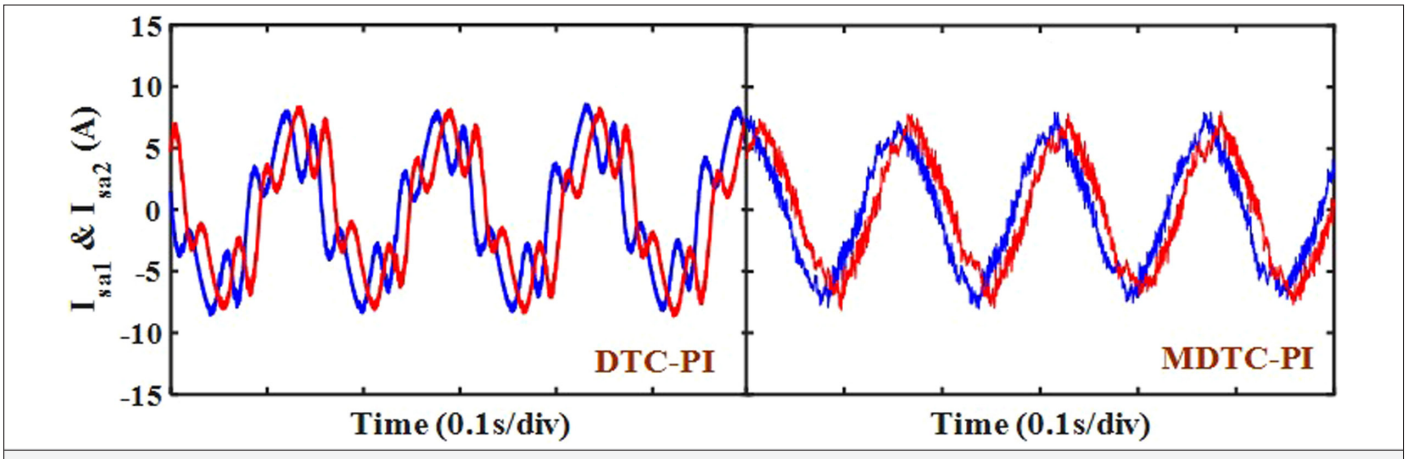

Fig. 10. Phase currents.

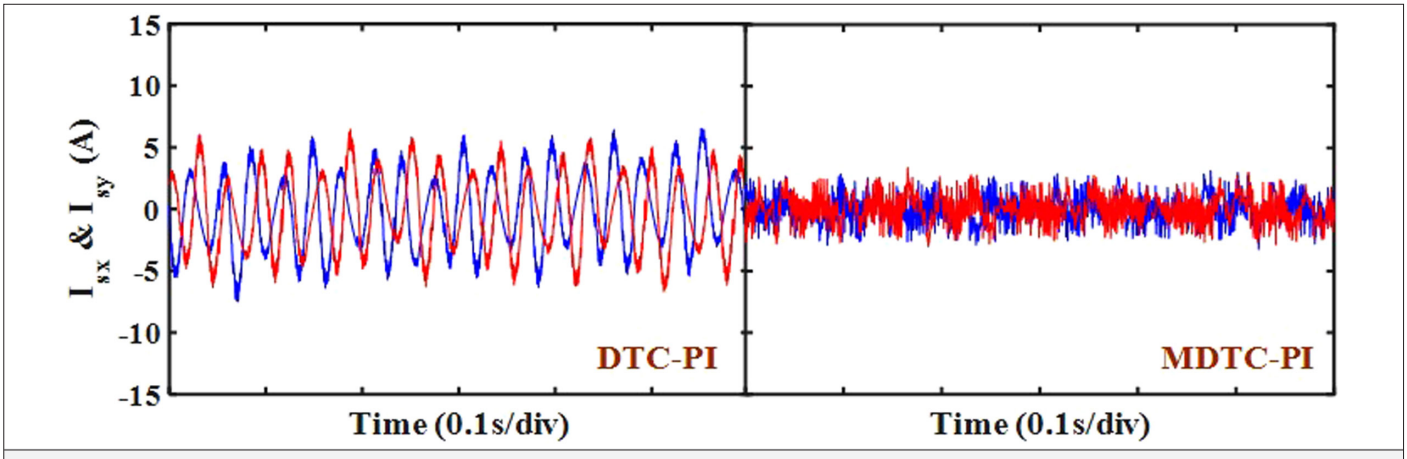

Fig. 11. Currents in x–y subspace.

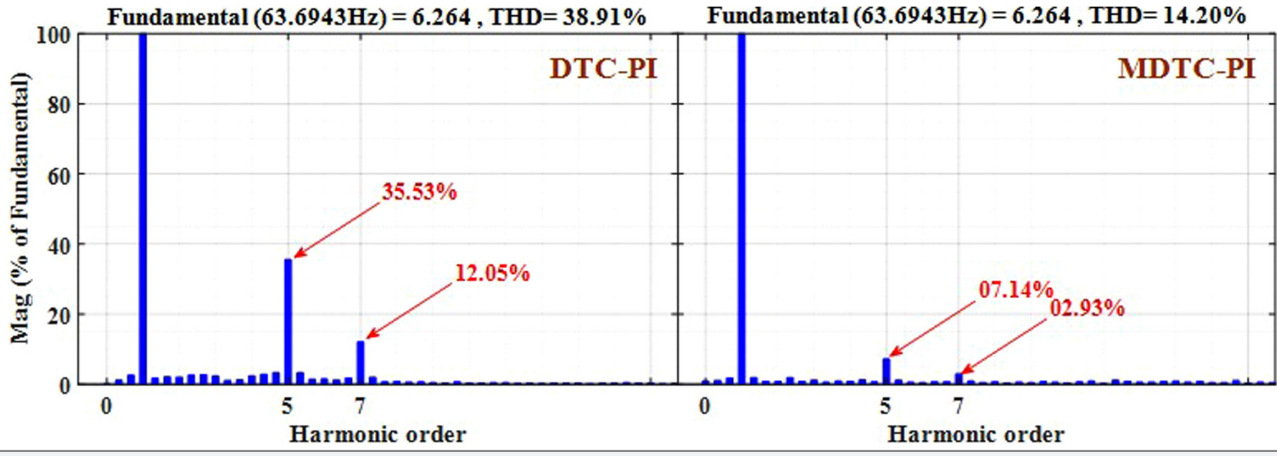

Fig. 12. Phase current harmonic spectrum.

Fig. 10, it is obvious that the phase currents of the DSIM by used DTC-PI have a non-sinusoidal current form. Moreover, Fig. 11 shows significant harmonic currents caused by the uncontrolled stator flux in the (x–y) subspace. Fig. 12 shows clearly that the modified MDTC-PI based on the two-step process can significantly reduce THD from 38.91% to 14.20% compared to the DTC-PI, leading to a purely sinusoidal current form and a significant minimization of harmonic currents.

Table III shows the THD of the current of the DSIM motor for the different DTC techniques studied in this paper. Simulations were carried out at a constant speed of 100 rad/s with different load torque values ranging from 10 Nm to 25 Nm. The five proposed MDTC-ROFrPI show that the THD can vary by ±2% from the THD value of the MDTC-PI. Furthermore, the MDTC-ROFrPI proposed-3 demonstrates that it can reduce THD compared with the other methods, showing that the choice of $\alpha = 0.3$ can bring improvements in terms of harmonic minimization compared with the other α values (0.1, 0.2, 0.4, and 0.5).

TABLE III. QUANTITATIVE THD OF PHASE CURRENT

	Load Torque		
Different Techniques	**10 Nm**	**20 Nm**	**25 Nm**
DTC-PI	77.86%	38.91%	32.66%
MDTC-PI	31.06%	14.20%	12.09%
MDTC-ROFrPI proposed-1	31.59%	12.49%	11.76%
MDTC-ROFrPI proposed-2	32.14%	14.63%	10.24%
MDTC-ROFrPI proposed-3	**29.81%**	**12.23%**	**10.17%**
MDTC-ROFrPI proposed-4	33.19%	14.27%	12.18%
MDTC-ROFrPI proposed-5	31.29%	13.57%	12.20%

DTC-PI, classical direct torque control with classic PI controller; MDTC-PI, modified direct torque control with classic PI controller; MDTC-ROFrPI proposed, proposed reduced-order fractionalized controller with modified direct torque control.
The values in bold are indicate the importance of the results obtained for the proposed techniques.

Comparative analysis of the different techniques proposed for the direct torque control of DSIM is carried out under other operating conditions. Table IV illustrates the torque ripples of several DTC strategies, calculated according to paper [19] using the root-mean-square error method. The rotor speed remains constant at 100 rad/s, while the load torque varies by 10 Nm, 20 Nm, and 25 Nm. The comparison shows that the proposed MDTC-ROFrPI-3 can slightly reduce torque ripples compared to MDTC-PI and the other proposed techniques over the whole torque variation range.

To compare the performance of the FrPI in the speed regulator loop with a conventional PI controller, a comparative stability analysis was conducted to improve the robustness of the DTC applied to the DSIM drive system. The reference speed is stabilized at 100 rad/s, and the load torque is set at 10 Nm. Fig. 13 compares the speed response to attain its stable speed with the maximum overshoot percentage, the rise time (for a tolerance of 10% to 90%), and the settling time (for a tolerance of 2%), while the quantitative results are presented in Table V. It is clear that the speed response for the proposed MDTC-ROFrPI-5, proposed MDTC-ROFrPI-4 and proposed MDTC-ROFrPI-3 quickly attain the reference with an overshoot of 0.7064, 0.7363, and

TABLE IV. QUANTIFICATION OF TORQUE RIPPLES IN SPEED OF 100 RAD/S FOR DIFFERENT LOAD TORQUE VALUES

	Load Torque		
Different Techniques	**10 Nm**	**20 Nm**	**25 Nm**
MDTC-PI	0.4209 Nm	0.3237 Nm	0.2552 Nm
MDTC-ROFrPI proposed-1	04212 Nm	0.3130 Nm	0.2572 Nm
MDTC-ROFrPI proposed-2	0.4178 Nm	0.3406 Nm	0.2628 Nm
MDTC-ROFrPI proposed-3	**0.4108 Nm**	**0.3014 Nm**	**0.2432 Nm**
MDTC-ROFrPI proposed-4	0.4123 Nm	0.3144 Nm	0.2603 Nm
MDTC-ROFrPI proposed-5	0.4111 Nm	0.3247 Nm	0.2552 Nm

MDTC-PI, modified direct torque control with classic PI controller; MDTC-ROFrPI proposed, proposed reduced-order fractionalized controller with modified direct torque control.
The values in bold are indicate the importance of the results obtained for the proposed techniques.

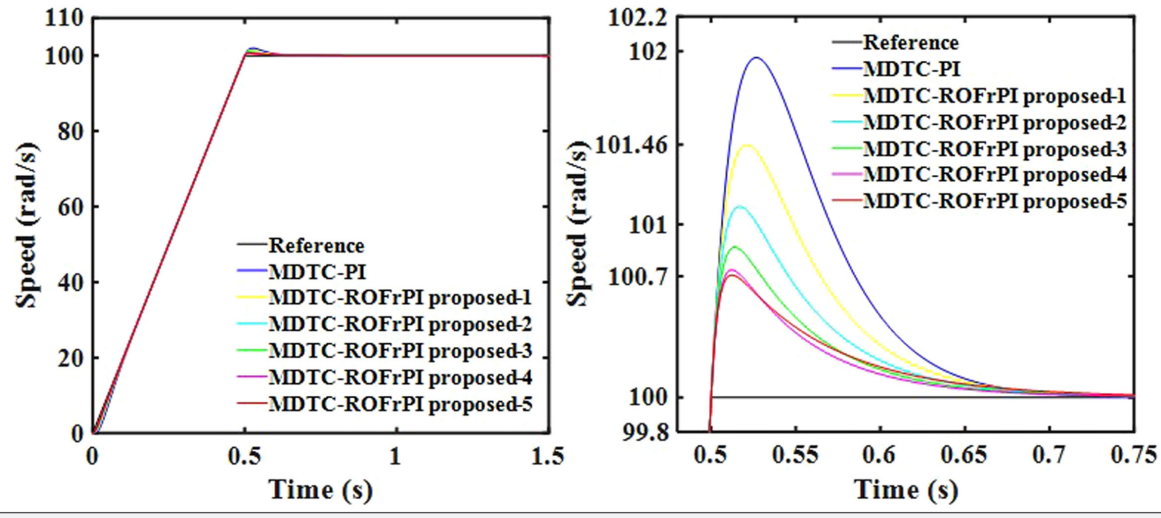

Fig. 13. Comparative study between the different MDTC-ROFrPI techniques proposed and MDTC-PI with a speed of 100 rad/s and a constant load of 10 Nm.

TABLE V. TRANSIENT RESPONSE RESULTS FOR DIFFERENT TECHNIQUES (SPEED: 100 RAD/S, TORQUE: 10 NM).

Different Techniques	Overshoot (%)	Settling Time (Seconds)	Rise Time (Seconds)
MDTC-PI	1.9630	0.6468	0.4221
MDTC-ROFrPI proposed-1	1.4606	0.5920	0.4212
MDTC-ROFrPI proposed-2	1.1032	0.5920	0.4208
MDTC-ROFrPI proposed-3	**0.8669**	0.5920	0.4206
MDTC-ROFrPI proposed-4	**0.7363**	0.5920	0.4205
MDTC-ROFrPI proposed-5	**0.7064**	0.5920	0.4205

MDTC-PI, modified direct torque control with classic PI controller; MDTC-ROFrPI proposed, proposed reduced-order fractionalized controller with modified direct torque control.
The values in bold are indicate the importance of the results obtained for the proposed techniques.

0.8669, respectively, compared to the other DTC strategies. In addition, it is essential to note that performance improves considerably for different values of $\alpha = 0.1$ (MDTC-ROFrPI proposed-1) and $\alpha = 0.2$ (MDTC-ROFrPI proposed-2) compared to MDTC-PI.

It is essential to improve the torque transient response in DTC for the DSIM. Fig. 14 and Table VI present the simulation results of five proposed DTC strategies based on the FrPI (for $\alpha = 0.1$, 0.2, 0.3, 0.4, and 0.5), compared with the conventional PI controller (with $\alpha = 1$), when the load torque undergoes an abrupt transition from 10 Nm to 20 Nm while maintaining a constant speed at 100 rad/s. It is clear that the proposed MDTC-ROFrPI, when used with the reduced-order FrPI using the Matsuda approximation in the speed regulator loop, has the shortest settling and rise times with minimum overshoot. The superiority of the approach using the FrPI for $\alpha = 0.5$ (MDTC-ROFrPI proposed-5) is evident, as it outperforms not only the conventional PI controller but also the other α values proposed in this paper.

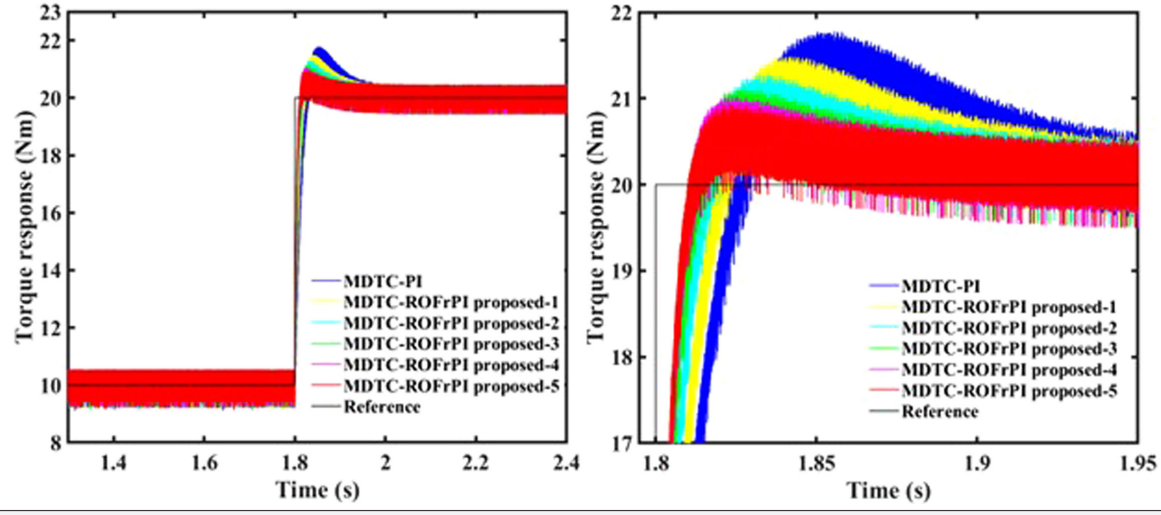

Fig. 14. Responses to external disturbances using different DTC strategies for an external load (10 Nm) is added at time 1.8 seconds with a speed of 100 rad/s.

TABLE VI. TRANSIENT RESPONSE RESULTS FOR DIFFERENT TECHNIQUES (SPEED: 100 RAD/S, TORQUE: 10 NM TO 20 NM)

Different Techniques	Overshoot (%)	Settling Time (s)	Rise Time (s)
MDTC-PI	6.7640	0.1415	0.0195
MDTC-ROFrPI proposed-1	5.3923	0.1291	0.0149
MDTC-ROFrPI proposed-2	4.3594	0.1160	0.0115
MDTC-ROFrPI proposed-3	3.4679	0.0937	0.0093
MDTC-ROFrPI proposed-4	3.1342	0.0926	0.0078
MDTC-ROFrPI proposed-5	**2.4748**	**0.0823**	**0.0077**

MDTC-PI, modified direct torque control with classic PI controller; MDTC-ROFrPI proposed, proposed Reduced-Order Fractionalized Controller with Modified direct torque control.
The values in bold are indicate the importance of the results obtained for the proposed techniques.

V. CONCLUSION

This paper presents a DTC technique based on a modified switching table and a FrPI of DSIM drive system. In effect, the modified switching table of the DTC scheme allows to select the suitable voltage vectors in order to reduce the harmonic currents in the (x–y) subspace. In addition, the proposed fractionalized order controller in the DTC, based on a Matsuda approximation method, can improve the dynamic performance of the DSIM. Moreover, a reduced-order fractionalized proportional-integral controller has also been also developed and compared with the FrPI. The validation results indicate that the reduced-order fractionalized PI controller presents a promising solution for the DTC of DSIM drive system in terms of in transient response, reducing rise time, settling time, and overshoot.

Peer-review: Externally peer-reviewed.

Author Contributions: Concept – S.G., B.T.; Design – S.G.; Supervision – S.G., B.T.; Resources – S.G.; Materials – S.G.; Data Collection and/or Processing – S.G.; Analysis and/or Interpretation – S.G., K.N.; Literature Search – S.G., K.N.; Writing – S.G., B.T., A.I.; Critical Review – A.I., K.N.

Declaration of Interests: The authors have no conflict of interest to declare.

Funding: The authors declared that this study has received no financial support.

REFERENCES

1. E. Levi, "Multiphase electric machines for variable-speed applications," *IEEE Trans. Ind. Electron.*, vol. 55, no. 5, pp. 1893–1909, 2008. [CrossRef]
2. E. Levi, R. Bojoi, F. Profumo, H. A. Toliyat, and S. Williamson, "Mul tiphase induction motor drives—A technology status review," *IET Elect. Power Appl.*, vol. 4, no. 1, pp. 489–516, 2007.
3. S. Guedida, B. Tabbache, K. Nounou, and M. Benbouzid, "Direct torque control scheme for less harmonic currents and torque ripples for dual star induction motor," *Rev Roum. Sci. Tech.-Ser.*, Vol. 68, no. 4, 2023, pp. 331–338.
4. F. Barrero, and M. J. Duran, "Recent advances in the design, modeling, and control of multiphase machines—Part I," *IEEE Trans. Ind. Electron.*, vol. 63, no. 1, pp. 449–458, 2015. [CrossRef]
5. S. Guedida, B. Tabbache, K. M. S. Benzaoui, K. Nounou, and M. Nesri, "Novel speed sensorless DTC design for a five-phase induction motor with an intelligent fractional order controller based-MRAS estimator," *Power Electron. Drives*, vol. 9, no. 1, pp. 63–85, 2024. [CrossRef]
6. Y. Zhao, and T. A. Lipo, "Space vector PWM control of dual three-phase induction machine using vector space decomposition," *IEEE Trans. Ind. Appl.*, vol. 31, no. 5, pp. 1100–1109, 1995. [CrossRef]
7. D. Hadiouche, H. Razik, and A. Rezzoug, "On the modeling and design of dual-stator windings to minimize circulating harmonic currents for VSI fed AC machines," *IEEE Trans. Ind. Appl.*, vol. 40, no. 2, pp. 506–515, 2004. [CrossRef]
8. D. Hadiouche, L. Baghli, and A. Rezzoug, "Space-vector PWM techniques for dual three-phase ac machine: Analysis, performance evaluation, DSP implementation," *IEEE Trans. Ind. Appl.*, vol. 42, no. 4, pp. 1112–1122, 2006. [CrossRef]
9. B. Shao, Z. Q. Zhu, J. Feng, S. Guo, Y. Li, and W. Liao, "Compensation of selective current harmonics for switching-table-based direct torque control of dual three-phase PMSM drives," *IEEE Trans. Ind. Appl.*, vol. 57, no. 3, pp. 2505–2515, 2021. [CrossRef]
10. M. Nesri, K. Nounou, S. Guedida, M. F. Benkhoris, and, A. Houari, "Hybrid flatness-based control of dual star induction machine drive system for more electrical aircraft," *Power Electron. Drives*, vol. 9, 2024.
11. R. Bojoi, M. Lazzari, F. Profumo, and A. Tenconi, "Digital field-oriented control for dual three-phase induction motor drives," *IEEE Trans. Ind. Appl.*, vol. 39, no. 3, pp. 752–760, 2003. [CrossRef]
12. I. Takahashi, and T. Noguchi, "A new quick-response and high efficiency control strategy of an induction motor," *IEEE Trans. Ind. Appl.*, vol. IA22, no. 5, pp. 820–827, 1986.
13. K. Hatua, and V. T. Ranganathan, "Direct torque control schemes for split-phase induction machine," *IEEE Trans. Ind. Appl.*, vol. 41, no. 5, pp. 1243–1254, 2005. [CrossRef]
14. R. Bojoi, F. Farina, G. Griva, F. Profumo, and A. Tenconi, "Direct torque control for dual three-phase induction motor drives," *IEEE Trans. Ind. Appl.*, vol. 41, no. 6, pp. 1627–1636, 2005. [CrossRef]
15. A. Taheri, A. Rahmati, and S. Kaboli, "Comparison of efficiency for different switching tables in six-phase induction motor DTC drive," *J. Power Electron.*, vol. 12, no. 1, pp. 128–135, 2012. [CrossRef]
16. Y. Gao, and L. Parsa, "Modified direct torque control of five-phase permanent magnet synchronous motor drives," Twenty Second Annual IEEE Applied Power Electronics Conf. APEC 2007, 2007, pp. 1428–1433. [CrossRef]
17. Y. N. Tatte, and M. V. Aware, "Direct torque control of five-phase induction motor with common-mode voltage and current harmonics reduction," *IEEE Trans. Power Electron.*, vol. 32, no. 11, pp. 8644–8654, 2016. [CrossRef]
18. Y. N. Tatte, and M. V. Aware, "Torque ripple and harmonic current reduction in a three-level inverter-fed direct-torque-controlled five-phase induction motor," *IEEE Trans. Ind. Electron.*, vol. 64, no. 7, pp. 5265–5275, 2017. [CrossRef]
19. Y. Ren, and Z. Q. Zhu, "Enhancement of steady-state performance in direct-torque-controlled dual three-phase permanent-magnet synchronous machine drives with modified switching table," *IEEE Trans. Ind. Electron.*, vol. 62, no. 6, pp. 3338–3350, 2014. [CrossRef]
20. B. Shao *et al.*, "Improved direct torque control method for dual-three-phase permanent-magnet synchronous machines with back EMF harmonics," *IEEE Trans. Ind. Electron.*, vol. 68, no. 10, pp. 9319–9333, 2020. [CrossRef]
21. M. H. Holakooie, G. Iwanski, and T. Miazga, "Switching-table-based direct torque control of six-phase drives with x-y current regulation," *IEEE Trans. Ind. Electron.*, vol. 69, no. 12, pp. 11890–11902, 2022. [CrossRef]
22. Y. Luo, K. Yang, and Y. Zheng, "Feedback linearization based direct torque control for asymmetrical six-phase PMSM motor with back EMF harmonics compensation," *IEEE J. Emerg. Sel. Top. Power Electron.*, vol. 11, no. 5, 5145–5155, 2023. [CrossRef]
23. K. D. Hoang, Y. Ren, Z. Q. Zhu, and M. Foster, "Modified switching-table strategy for reduction of current harmonics in direct torque controlled dual-three-phase permanent magnet synchronous machine drives," *IET Electr. Power Appl.*, vol. 9, no. 1, pp. 10–19, 2015. [CrossRef]
24. D. Valério, and J. S. Da Costa, "Tuning of fractional PID controllers with Ziegler–Nichols-type rules," *Signal Process.*, vol. 86, no. 10, pp. 2771–2784, 2006. [CrossRef]
25. A. N. Karanam, B. Shaw, and J. R. Nayak, "A combined fractional order proportional integral derivative controller for automatic generation control integrated with wind and small hydropower plant using crow search algorithm," *Electrica*, vol. 23, no. 3, p., 2023. [CrossRef]

26. I. Podlubny, "Fractional-order systems and PI/sup/spl lambda//D/sup/spl mu//-controllers," *IEEE Trans. Autom. Control*, vol. 44, no. 1, pp. 208–214, 1999. [CrossRef]
27. M. Nesri, H. Benkadi, K. Nounou, G. Sifelislam, and M. F. Benkhoris, "Fault tolerant control of a dual star induction machine drive system using hybrid fractional controller," *Power Electron. Drives*, vol. 9, no. 1, pp. 161–175, 2024. [CrossRef]
28. A. Idir, L. Canale, Y. Bensafia, and K. Khettab, "Design and robust performance analysis of low-order approximation of fractional PID controller based on an IABC algorithm for an automatic voltage regulator system," *Energies*, vol. 15, no. 23, p. 8973, 2022. [CrossRef]
29. A. Idir, Y. Bensafia, K. Khettab, and L. Canal, "Performance improvement of aircraft pitch angle control using a new reduced order fractionalized PID controller," *Asian J. Control*, vol. 25, no. 4, pp. 2588–2603, 2023. [CrossRef]
30. S. Ladaci, J. J. Loiseau, and A. Charef, "Fractional order adaptive high-gain controllers for a class of linear systems," *Commun. Nonlinear Sci. Numer. Simul.*, vol.13, no. 4, pp. 707–714, 2008. [CrossRef]
31. Y. Bensafia, K. Khettab, and A. Idir, "An improved robust fractionalized PID controller for a class of fractional-order systems with measurement noise," *Int. J. Intell. Eng. Syst.*, vol. 11, no. 2, 200–207, 2022. [CrossRef]
32. J. Sabatier, A. Oustaloup, A. G. Iturricha, and F. Levron, "CRONE control of continuous linear time periodic systems: Application to a testing bench," *ISA Trans.*, vol. 42, no. 3, pp. 421–436, 2003. [CrossRef]
33. R. Garrappa, "A Grunwald–Letnikov scheme for fractional operators of Havriliak–Negami type," *Math. Comput. Sci. Eng. Ser.*, Vol. 34, 2014, pp. 70–76.
34. K. Matsuda, and H. Fujii, "H (infinity) optimized wave-absorbing control-Analytical and experimental results," *J. Guid. Control Dyn.*, vol. 16, no. 6, pp. 1146–1153, 1993. [CrossRef]

Sifelislam Guedida was born in Algeria. In 2017, he obtained a master's degree in automation and industrial informatics from the Ècole Supérieur Ali CHABATI in Algiers, Algeria. He is currently working as a PhD student in UER electrotechnique at the Ecole Militaire Polytechnique in Algeria. His research interests include the control of multiphase machines and power electronics. Email: guedida.sifelislam@gmail.com.

Bekheira Tabbache received the BTech, MTech, and PhD degrees in electrical engineering, from the Polytechnic Military Academy, Algiers, Algeria, in 2003, 2007, and 2013, respectively. Since 2004, he has been with the electrical engineering department of the Polytechnic Military Academy, Algiers, Algeria. His current research interests are control of electrical drives, power electronics, and fault-tolerant control. Email: laid_tabache@yahoo.com.

Kamal Nounou was born in Jijel, Algeria, in 1983. received the Engineer degree, the M.Sc and Ph.D. degrees in electrical engineering from the Ecole Militaire Polytechnique (EMP), Algiers, Algeria, in 2007, 2014 and 2020, respectively. His research interests include fault tolerant control, multiphase machines, and drives. Email: nounou.kamal18@gmail.com.

Abdelhakim Idir graduated from Bejaia University in 2003 with an Engineer degree in Control systems. He received his Magister degree in control from Setif University in 2006, a doctorate and HDR degrees in electrical engineering from University M'Hamed Bougara in Boumerdes, Algeria, in 2015 and 2018, respectively. He is currently a Professor at Algeria's Mohamed Boudiaf of M'sila University (UMBM). At the Laboratory of Applied Automatics, he directs the control system research teams (LAA). His current research interests include fractional system modeling, simulation, and control, fractional PID control, AC drives, and renewable energy. He can be contacted at e-mail: abdelhakim.idir@univ-msila.dz.